Chemistry of Metals and Alloys

Chem. Met. Alloys 6 (2013) 130-143
Ivan Franko National University of Lviv
www.chemetal-journal.org

Isotope effect on structural transitions in $Y_{0.9}Gd_{0.1}Fe_2(H_zD_{1-z})_{4.2}$ compounds

Valérie PAUL-BONCOUR[1]*, Svetlana VOYSHNIS[1], Karine PROVOST[1], Jean-Claude CRIVELLO[1]

[1] *Institut de Chimie et des Matériaux de Paris Est, CMTR, CNRS-UPEC, UMR 7182, 2-8 rue Henri Dunant, 94320 Thiais Cedex, France*
* *Corresponding author. Tel.: +33-1-49781207; fax: +33-1-49781203; e-mail: paulbon@icmpe.cnrs.fr*

Received September 20, 2013; accepted December 25, 2013; available on-line August 30, 2014

$Y_{0.9}Gd_{0.1}Fe_2(H_zD_{1-z})_{4.2}$ compounds crystallize in a monoclinic structure at room temperature, with an increase of the cell parameters *versus* the H content. These compounds undergo a ferro-antiferromagnetic first-order transition, the transition temperature of which increases from 98 to 144 K for *z* going from 0 to 1, due to a strong magnetovolumic effect. Above room temperature (290-340 K), they display an order-disorder (O-D) transition from monoclinic towards a cubic structure, which has been studied by DSC and XRD *versus* temperature. This transition occurs *via* the presence of an intermediate phase, the structure of which depends on the H content. For $z = 0$ and 0.5 the intermediate phase is monoclinic, whereas an orthorhombic phase is observed for $z = 0.75$ and 1. In addition, for the H-rich compounds the orthorhombic phase disappears at a much lower temperature upon cooling than it appears upon heating. DFT band structure calculations for YFe_2H_x compounds showed that for $4 < x < 4.5$, although the monoclinic phase is the more stable one, the energy of formation of the orthorhombic phase is only 0.1 kJ higher. For $4.5 < x \leq 5$ the orthorhombic phase becomes more stable. The sensitivity of the O-D transition to the H/D content could be related to a volume effect. At higher temperatures ($T > 400$ K), the thermal desorption studied by TGA shows a multipeak behavior that is not sensitive to the (H, D) isotope effect.

Laves phases / Isotope effect / X-ray diffraction / Order-disorder transition / DFT calculation

Introduction

Hydrogen absorption can strongly modify the magnetic properties of *R*-*T* (*R* = rare earth, *T* = transition metal) intermetallic compounds due to cell volume expansion and changes in the electronic structure [1]. YFe_2 can absorb up to 5 H/f.u. and form hydrides or deuterides with different crystal structures [2-10]. Generally, H for D substitution has no significant influence on the magnetic properties of metal hydrides. However, it has been discovered that the magnetic properties of $YFe_2(H_zD_{1-z})_{4.2}$ compounds are very sensitive to the nature of the hydrogen isotope: the ferro-antiferromagnetic (F-AF) transition temperature $T_{F\text{-}AF}$ is shifted from 84 K to 131 K for *z* going from 0 to 1 [11,12]. This has been explained by the larger cell volume of $YFe_2H_{4.2}$ compared to that of $YFe_2D_{4.2}$, which induces a large magnetovolumic effect. $T_{F\text{-}AF}$ can also be modified by applying an external pressure [13], or by tuning the cell volume by the replacement of Y by another rare-earth element (*R* = Gd, Tb, Er) [14,15]. These compounds are interesting not only for this unusual isotope effect, but also because a large magnetocaloric effect is observed at the F-AF transition [16,17]. However, the transition temperature should be increased for magnetic refrigeration applications. This can be achieved by the substitution of Gd or Tb for Y, which induces a significant increase of the cell volume and $T_{F\text{-}AF}$.

In addition, $YFe_2D_{4.2}$ shows a particular structural transition in the room temperature range. Upon heating above 330 K, $YFe_2D_{4.2}$ undergoes an order-disorder (O-D) transition from a monoclinic (space group *C*2/*m*) towards a cubic (S.G. *Fd*-3*m*) structure, with an intermediate rhombohedral structure (S.G. *R*-3*m*) [10,13]. At low temperature the deuterium atoms are located in specific Y_2Fe_2 and YFe_3 interstitial sites. This induces a displacement of the metallic neighbors and a lowering of the crystal symmetry. Above a critical temperature $T_{O\text{-}D}$, the D atoms randomly move inside the different sites and an average cubic structure is observed. A study of the local order of $YFe_2D_{4.2}$ by a partial distribution function (PDF), obtained from neutron diffraction patterns measured below and above the O-D transition ($T_{O\text{-}D}$), temperature has shown that the local order

remains the same up to about 8 Å (*i.e.* inside one unit cell) and diverges for larger interatomic distances [10,18]. The PDF analysis has shown that each Fe atom is surrounded by 4 or 5 D atoms. In addition to the large isotope effect on the F-AF magnetic transition in the $Y_{1-y}Gd_yFe_2(D_{1-z}H_z)_{4.2(1)}$ compounds, we observed for the first time that the O-D transition is also isotope sensitive, even for small amounts of substituting Gd (y = 0.05 and 0.1).

We have undertaken a systematic study of the influence of substitution of both Gd for Y and H for D on the structural and magnetic properties of $Y_{1-y}Gd_yFe_2(D_{1-z}H_z)_{4.2(1)}$ compounds with the aim to improve their magnetocaloric properties and to better understand the O-D transition. In this work, we present the results obtained for one selected Gd concentration (y = 0.1). The $Y_{0.9}Gd_{0.1}Fe_2(H_zD_{1-z})_{4.2(1)}$ compounds were studied by ThermoGravimetric Analysis (TGA), Differential Scanning Calorimetry (DSC), X-Ray Diffraction (XRD), and magnetic measurements *versus* temperature. The isotope effect on both the magnetic and structural transitions will be discussed in comparison with the non-substituted $YFe_2(H_zD_{1-z})_{4.2}$ compounds. In complement to these experimental results, we have performed DFT calculations for YFe_2H_x compounds ($3.5 \leq x \leq 5$), in order to compare the phase stability of the hydride in different structures (cubic, monoclinic and orthorhombic) *versus* the H content.

Experimental

The $Y_{0.9}Gd_{0.1}Fe_2$ intermetallic compound was prepared by induction melting of the pure elements, followed by 3 weeks of annealing at 1100 K. The composition and homogeneity of the alloy were checked by X-ray powder diffraction (XRD) using a Bruker D8 diffractometer (Cu K_α radiation) and electron probe microanalysis (EPMA), as described in [19].

The $Y_{0.9}Gd_{0.1}Fe_2(H_zD_{1-z})_{4.2}$ samples were prepared by solid-gas reaction using a Sievert apparatus, as described in [19], then quenched into liquid nitrogen, and after that slowly heated under air to poison the surface and prevent gas desorption. The total (H, D) content corresponds to the one calculated by the volumetric method, before quenching into liquid nitrogen. The hydrogen/deuterium mixture was prepared by using two tanks filled with H_2 and D_2, respectively, and adjusting the pressure in each tank to obtain the wished H/D ratio. The two tanks were then opened to fill the hydrogenation bath and form a H/D mixture in the gas phase.

The samples were characterized by XRD at room temperature with a Bruker D8 diffractometer (Cu K_α), and the patterns refined with the fullprof code [20]. The order-disorder transitions were studied by XRD *versus* temperature with a Bruker D8 diffractometer equipped with a Vantec detector and an oven.

The thermal behavior was studied using a differential scanning calorimeter DSC Q100 from TA Instruments, under Ar flow and with a heating/cooling rate of 10 K/min. The (H, D) desorption was studied by thermogravimetric analysis (TGA) Setsys evolution from SETARAM, filled with argon.

The magnetization measurements were performed using a conventional Physical Properties Measurement System (PPMS) from Quantum Design with a maximum field of 90 kG.

Spin-polarized band structure calculations were made by using the DFT scheme implemented in the projector-augmented wave (PAW) method, performed with the VASP package [21,22]. The Generalized Gradient Approximation (GGA) was used with the Perdew and Wang functional [23]. A plane wave basis set with a cutoff energy of 600 eV and high-density k-point meshing were used in all the calculations, converging within 0.1 eV in total energy. The structural forces in the hydrides were first minimized by relaxing the cell parameters but keeping the initial symmetry of the structure, and then by relaxing the internal atomic positions.

The phase stability of YFe_2H_x hydrides crystallizing in three different structures was considered. The first structure is the cubic C15 (S.G. *Fd*-3*m* (227)), studied for $3 \leq x \leq 5$ with a step Δx of 0.5, and the cubic cell parameter a_C . The second structure is monoclinic (S.G. *P*1*c*1 (7)); it appears experimentally for x = 4.2(1) and was calculated for x = 3.25 to 4.75 with Δx = 0.25. From the cubic cell, the monoclinic structure is obtained by applying $a' = \sqrt{2}a_C/2$, $b' = \sqrt{2}a_C$, $c' = -a_C\cos\beta$, $\beta = 90 + \mathrm{Atan}(\sqrt{2}/2)$. The third structure, observed experimentally for x = 5, is orthorhombic (S.G. *Pmn*2$_1$ (31)), with $a'' = b'' = \sqrt{2}a_C/2$, $c' = a_C$. For all the studied compounds the hydrogen sites were chosen so that they reproduce the experimental site occupancies (position and preferences) found by neutron diffraction for a given x value [10,24,25]. H atoms were added or removed, taking into account the experimental occupancies, in order to tune the H content between 3 and 5.

Results and discussion

a) Experimental results

$Y_{0.9}Gd_{0.1}Fe_2$ is single phase and crystallizes in a cubic C15 structure with a = 7.364(1) Å.

Four $Y_{1-y}Gd_yFe_2(D_{1-z}H_z)_{4.2(1)}$ samples with different H/D ratios (z = 0, 0.5, 0.75, 1) were synthesized. Their XRD patterns showed a mixture of monoclinic (*C*2/*m*) and cubic (*Fd*-3*m*) phases, the cell parameters and relative weight percent of which are reported in Table 1. As an example, the refined pattern of $Y_{0.9}Gd_{0.1}Fe_2D_{4.3}$ is shown in Fig. 1 and the corresponding atomic positions of the monoclinic phase are reported in Table 2. The amount of

Table 1 Cell parameters of $Y_{0.9}Gd_{0.1}Fe_2(H_zD_{1-z})_{4.2}$ compounds at room temperature.

Compound	Space group	wt.%	*a* (Å)	*b* (Å)	*c* (Å)	*β* (°)	*V* (Å^3)	Δ*V*/*V* (%)
$Y_{0.9}Gd_{0.1}Fe_2D_{4.3}$	*C*2/*m*	65(1)	9.4399(3)	5.7456(2)	5.5119(2)	122.33(1)	252.607(15)	26.52
	Fd-3*m*	35(1)	7.992(1)				510.49(14)	27.83
$Y_{0.9}Gd_{0.1}Fe_2(D_{0.5}H_{0.5})_{4.1}$	*C*2/*m*	78(2)	9.4491(1)	5.7514(1)	5.5201(1)	122.34(1)	253.463(4)	26.99
	Fd-3*m*	22(2)	7.975(1)				507.13(16)	26.96
$Y_{0.9}Gd_{0.1}Fe_2(D_{0.75}H_{0.25})_{4.1}$	*C*2/*m*	65(2)	9.4551(3)	5.7561(2)	5.5241(2)	122.32(1)	254.056(14)	27.25
	Fd-3*m*	35(2)	8.005(1)				512.96(11)	28.45
$Y_{0.9}Gd_{0.1}Fe_2H_{4.4}$	*C*2/*m*	75(1)	9.4589(2)	5.7581(2)	5.5249(2)	122.33(1)	254.271(1)	27.36
	Fd-3*m*	25(1)	7.9969(6)				511.424(7)	28.07

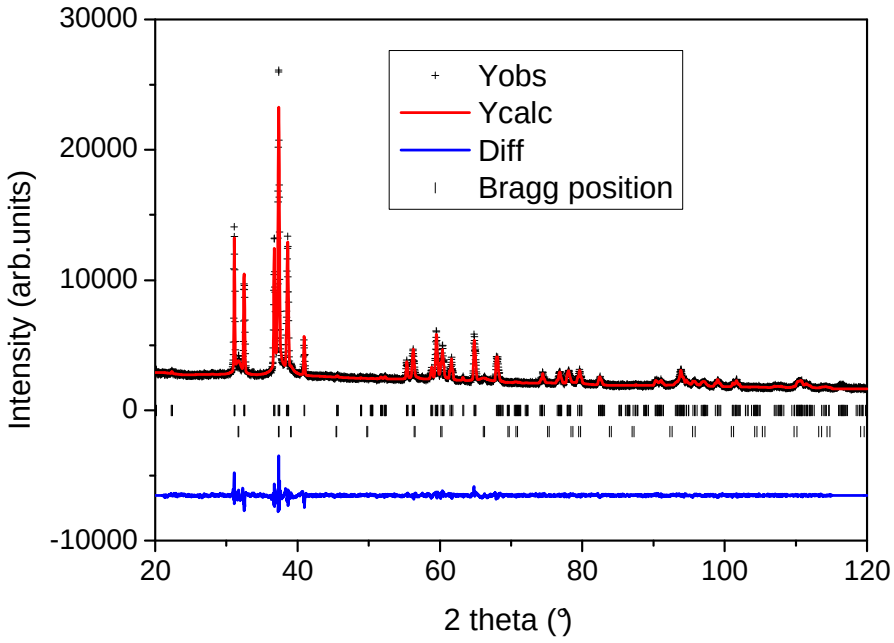

Fig. 1 Refined XRD pattern of $Y_{0.9}Gd_{0.1}Fe_2D_{4.3}$.

monoclinic phase varies between 65 and 78 wt%. The *a*, *b*, *c* parameters of the monoclinic phase increase with increasing *z*, whereas the monoclinic angle *β* remains constant. The cell volume *V* increases with increasing *z*, as for the non-substituted compounds. The $V = f(z)$ curve can be refined by a linear fit (V_0= 252.63(10) Å^3, *B*= 1.73(15) Å^3, R_{fit} =0.976) which can be compared with that of $YFe_2D_{4.2}$ (V_0= 251.48(6) Å^3, *B* = 1.99(9) Å^3, R_{fit} =0.996) [12]. The increase of the cell volume was attributed to the larger amplitude of the zero point vibration of H atoms compared to D atoms, inside interstitial sites surrounded by heavy atoms [26].

The cell volume of the cubic phase is not clearly related to the H/D ratio, and taking into account the twice larger number of atoms by unit cell ($Z = 8$ for the cubic phase, $Z = 4$ for the monoclinic phase), the volume is equal to or larger than the volume of the corresponding monoclinic cell.

The difference of the volumetric behavior between the monoclinic and cubic phases is related to their different hydrogenation properties. For all $Y_{1-y}R_yFe_2(H/D)_x$ compounds, H/D ordering occurs for well defined H or D contents, accompanied by a lowering of the crystal symmetry below the O-D transition temperature. For the intermediate *x* ranges no ordering of H/D occurs, and the phase always presents the *Fd*-3*m* symmetry, whatever the temperature. These cubic phases can be understood as H/D solid solutions in the host compound. Therefore the cell parameters of the cubic phase depend on the total (H, D) content as well as on the H/D ratio, and can vary randomly from one sample to another.

The DSC curves measured upon cooling and heating for the four samples, display peaks corresponding to three different ranges of temperature, as shown in Fig. 2 for $Y_{0.9}Gd_{0.1}Fe_2H_{4.4}$: i) at low temperature the weak peaks are due to the change of volume associated with the magnetic transition,

Table 2 Refined atomic positions of the monoclinic phase (space group *C*2/*m*) in $Y_{0.9}Gd_{0.1}Fe_2D_{4.3}$. The Bragg factor for this phase is R_F = 4.4%.

Atom	Wyckoff position	*x*	*y*	*z*	*B* (Å^2)
Y,Gd	4*i*	0.8692(4)	0	0.1337(7)	0.21(5)
Fe1	2*d*	0	½	½	0.14(6)
Fe2	2*b*	0	½	0	0.14(6)
Fe3	4*f*	¼	¼	½	0.14(6)

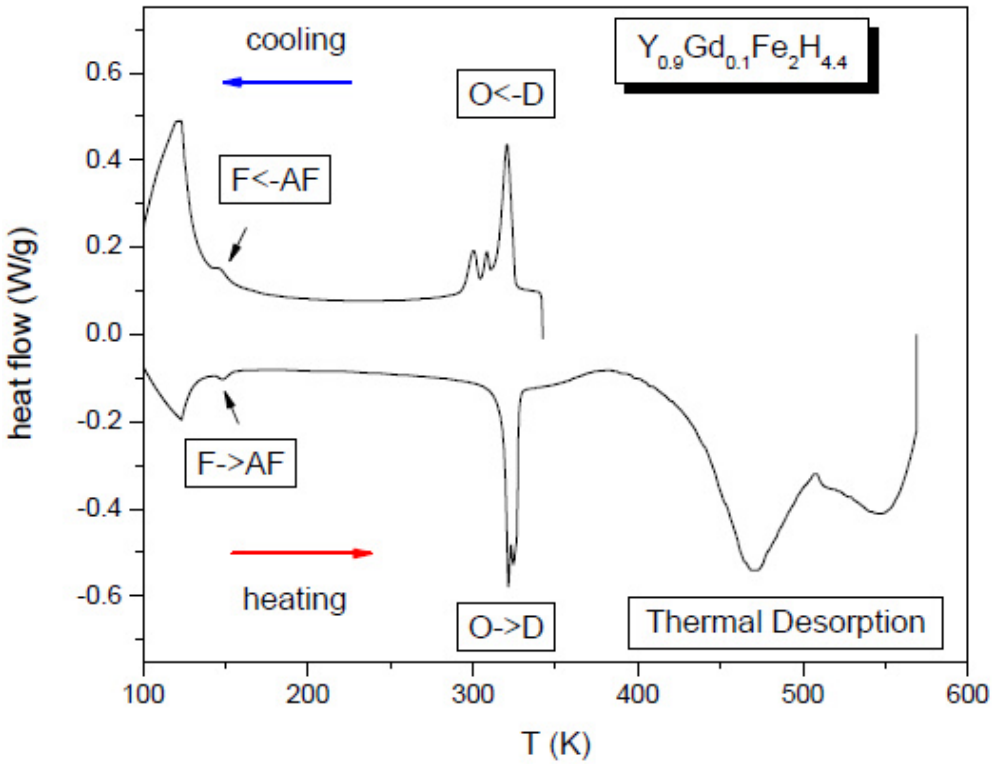

Fig. 2 Full DSC curve of $Y_{0.9}Gd_{0.1}Fe_2H_{4.4}$.

ii) near room temperature, the peaks can be attributed to the order-disorder structural transition, iii) at higher temperature the broad peaks are related to the thermodesorption process.

Experimental results will be presented to follow the different types of transition observed upon increasing the temperature: i) the magnetic transition at low *T*, ii) the order-disorder transition close to room temperature, iii) the thermal desorption at high temperature.

i) Magnetic transition

Magnetization *versus* field *M*(*B*) and temperature *M*(*T*) curves were measured for the four samples. The *M*(*T*) and *M*(*B*) curves of $Y_{0.9}Gd_{0.1}Fe_2D_{4.3}$ are displayed in Fig. 3.

As for $YFe_2D_{4.2}$, the sharp decrease of the magnetization around 100 K can be attributed to the F-AF transition (Fig. 3a). The *M*(*B*) curves (Fig. 3b) show different magnetic behavior depending on the temperature. At 2 K, the $M_{2K}(B)$ curves show ferromagnetic behavior with a spontaneous magnetization of 3.15(1) μ_B. Between 100 K and 150 K, the *M*(*B*) curves display metamagnetic behavior with a transition field B_{trans} determined by the maximum of the derivative curve for each temperature. B_{trans} increases linearly with increasing *T* and its extrapolation to zero field allows determining the transition temperature without field (denoted T_{M0} as in previous works): T_{M0} = 98 K for *z* = 0. Between 200 K and 300 K, the material is paramagnetic, with weak spontaneous magnetization (0.13 μ_B at 300 K).

Similar magnetic behavior was observed for all of the compounds. The spontaneous magnetization (M_{spont}) extrapolated to zero field varies between 3.08(1) and 3.30(1) μ_B/f.u. (Table 3). These values are smaller than for the non-substituted compounds, and, assuming antiparallel coupling of Fe and Gd and the same value of the Fe moment, one can estimate for *z* = 0, 0.5 and 0.75 a Gd moment close to 6.0(6) μ_B, slightly smaller than the Gd free ion value (7 μ_B).

Table 3 Magnetic parameters (T_{M0}: temperature at B = 0 G, dB/dT slope, M_{spont}: spontaneous magnetization) and TGA results (H+D content, transition temperatures).

Compound	T_{M0} (K)	dB/dT (kG/K)	M_{spont} (2 K) (μ_B)	C_{des}(H, D)/f.u. (TGA)	T_1 (K)	T_2 (K)	T_3 (K)
$Y_{0.9}Gd_{0.1}Fe_2D_{4.3}$	98.0(2)	1.93(1)	3.15(1)	4.0(1)	432.5	450.0	498.4
$Y_{0.9}Gd_{0.1}Fe_2(D_{0.5}H_{0.5})_{4.1}$	125.8(2)	1.47(1)	3.30(1)	3.9(1)	432.4	481.8 [a]	
$Y_{0.9}Gd_{0.1}Fe_2(D_{0.75}H_{0.25})_{4.1}$	129.3(2)	1.13(1)	3.23(1)	3.7(3)	428.5	445.7	496.8
$Y_{0.9}Gd_{0.1}Fe_2H_{4.4}$	144.0(5)	0.99(1)	3.08(1)	4.0(1)	434.0	445.0	515.0

[a] Peaks 2 and 3 are not well separated and an average value was obtained.

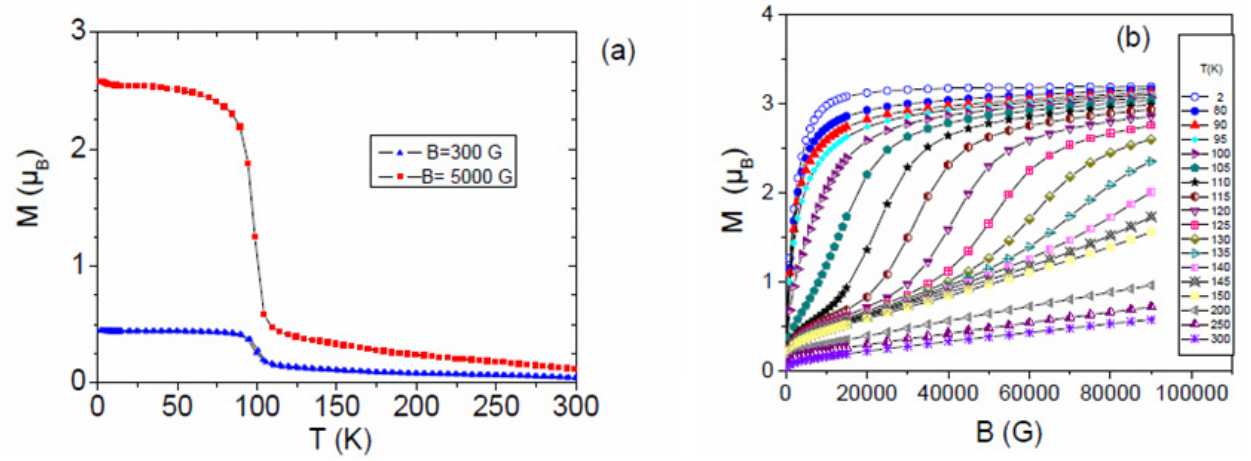

Fig. 3 Magnetization of $Y_{0.9}Gd_{0.1}Fe_2D_{4.3}$ *versus* temperature (a) and field (b).

The difference of M_{spont} between $Y_{0.9}Gd_{0.1}Fe_2H_{4.3}$ and $YFe_2H_{4.2}$ is larger (close to 1 μ_B) than for the other compounds; this value will lead to a too large Gd moment, compared to the free ion value, and experimental errors have to be taken into account.

For all of the compounds the evolution of B_{trans} *versus* T (Fig. 4) shows that: i) T_{M0} increases with increasing z, ii) the dB/dT slope decreases with increasing z (Table 3). These results confirm the large isotope effect on the magnetic properties of these compounds, as already observed for the non-substituted compounds.

ii) Order-disorder transition

The DSC curves corresponding to the O-D structural transformations between 290 and 340 K are presented in Fig. 5 for the four compounds. Upon heating, $Y_{0.9}Gd_{0.1}Fe_2D_{4.3}$ displays one large peak at 330.2 K (T_1) followed by two small peaks at 331.2 (T_2) and 334.7 K (T_3). An almost symmetric behavior is observed upon cooling, with a shift of the maximum peak positions of between 2 and 4 K to lower temperatures. It can be noted that the onset temperature of the main peak (T_1, $T_{1'}$) is 328 K upon both heating and cooling.

$Y_{0.9}Gd_{0.1}Fe_2(D_{0.5}H_{0.5})_{4.1}$ mainly shows two large peaks upon heating and cooling, with a temperature difference $\Delta T_{1\text{-}3}$ = 3 K and $\Delta T_{1'\text{-}3'}$ = 5 K. The peak temperatures are about 4±1 K lower than those of the corresponding peaks of the deuterides.

$Y_{0.9}Gd_{0.1}Fe_2(D_{0.25}H_{0.75})_{4.1}$ and $Y_{0.9}Gd_{0.1}Fe_2H_{4.4}$ display two or three peaks upon heating, at lower temperatures than for z = 0 and z = 0.5. A decrease of 8.8 K/H atom for T_1 and 8 K/H atom for T_3 is observed. The difference between T_1 and T_3 remains similar to that observed for the two previous samples ($\Delta T_{1\text{-}3}$ = 3 and 5 K for z = 0.75 and 1, respectively). But, upon cooling the difference between $T_{1'}$ and $T_{3'}$ extends over a much broader temperature range ($\Delta T_{1'\text{-}3'}$ = 14.8 and 20.4 K for z = 0.75 and 1, respectively). A plot of the peak maximum temperatures (T_n) is reported in Fig. 6. Upon heating (red lines), the decrease of T_1 and T_3 is continuous and remains moderate. Upon cooling (blue lines), a marked change is observed in the $\Delta T/\Delta z$ slope for $T_{1'}$ at z = 0.5: 8.2 K/H atom for z = 0 to 0.5 and 45 K/H atom for z = 0.5 to 1.

In order to understand the origin of the difference of the O-D structural behavior between the D-rich samples (z = 0 and 0.5) and the H-rich samples (z = 0.75 and 1), XRD patterns were recorded from 298 to 343 K upon heating and cooling.

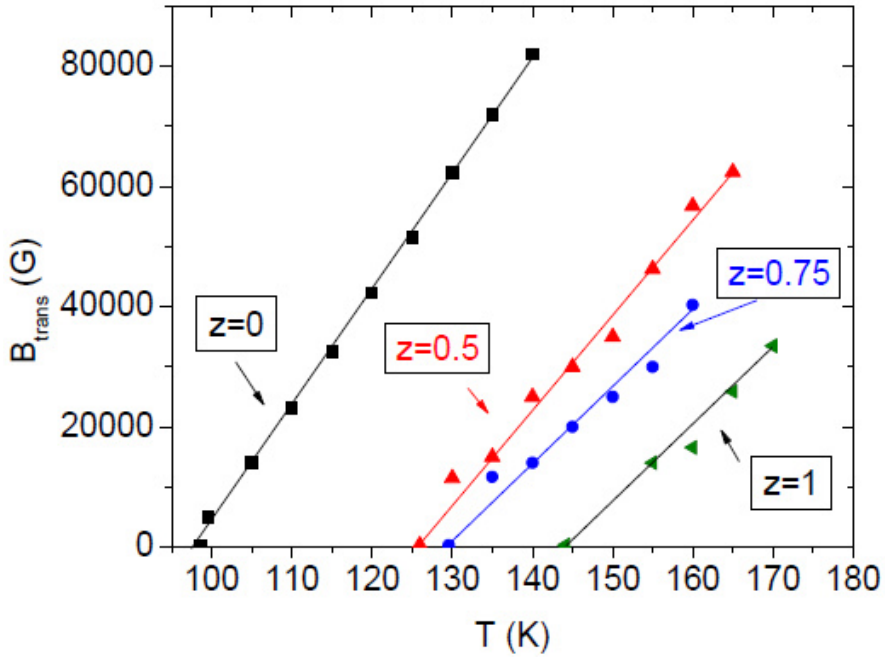

Fig. 4 Transition field *versus* temperature for $Y_{0.9}Gd_{0.1}Fe_2(H_zD_{1-z})_{4.2}$.

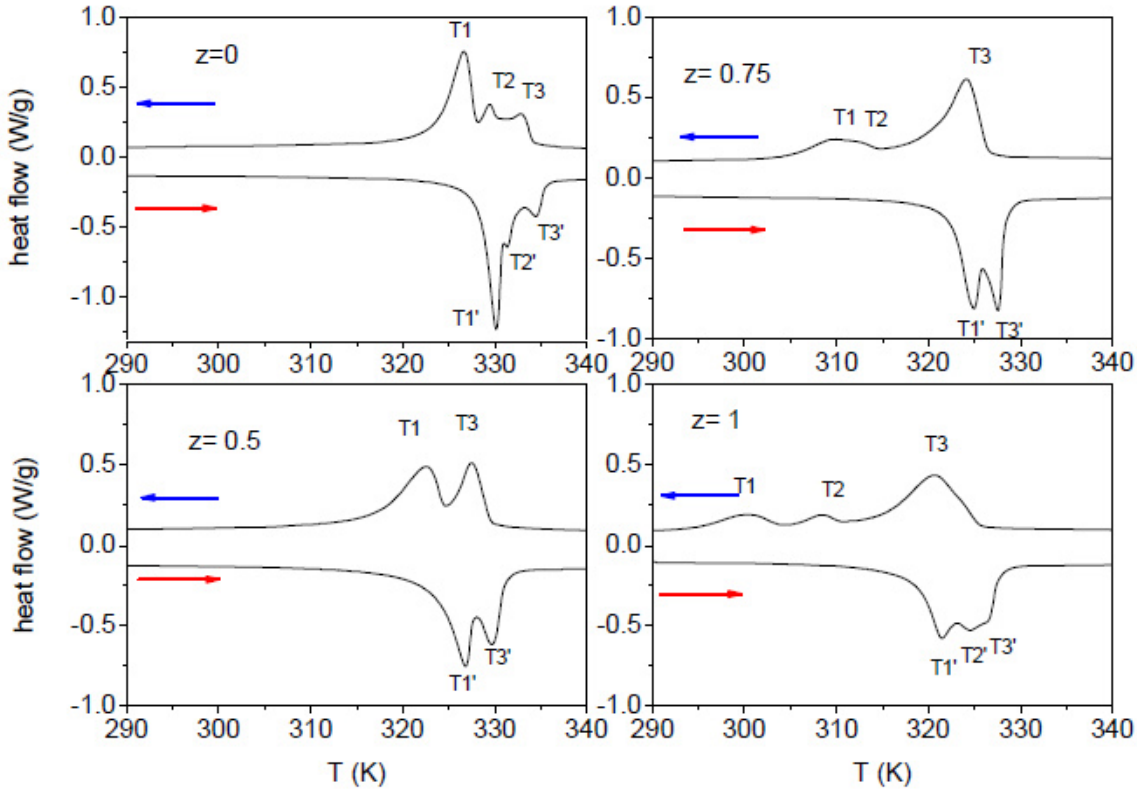

Fig. 5 DSC curves of $Y_{0.9}Gd_{0.1}Fe_2(H_zD_{1-z})_{4.2}$ compounds, zoomed between 290 and 340 K to show the O-D transitions. The arrows indicate heating (→) and cooling (←). Each peak is labeled by *Tn* (heating) or *Tn'* (cooling) with *n* = 1 to 3.

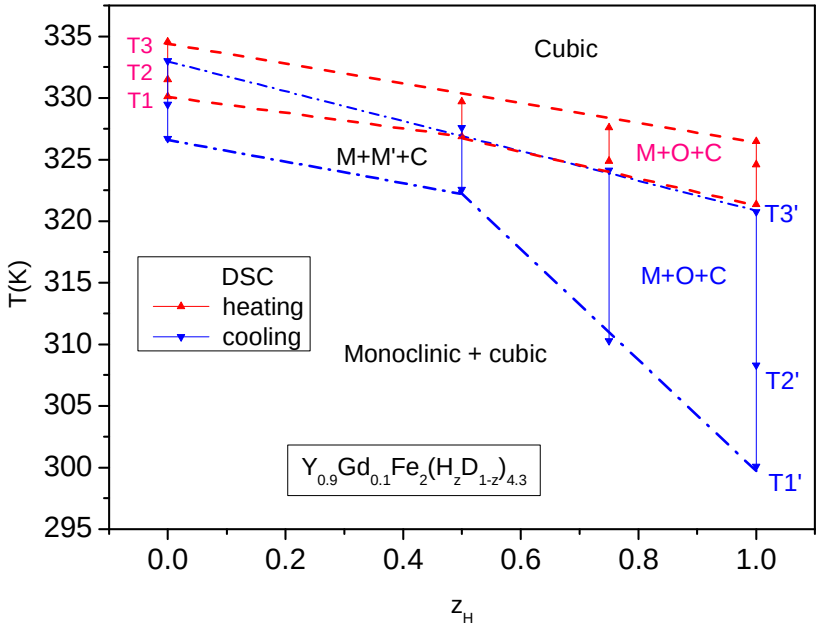

Fig. 6 Transition temperatures (DSC peak maxima) *versus* H content for $Y_{0.9}Gd_{0.1}Fe_2(H_zD_{1-z})_{4.2}$ compounds. The results of XRD *versus* temperature have been added to explain which structural transition is occurring.

The evolution of the diffraction patterns of $Y_{0.9}Gd_{0.1}Fe_2D_{4.3}$ and $Y_{0.9}Gd_{0.1}Fe_2(D_{0.25}H_{0.75})_{4.1}$ *versus* temperature is reported in Figs. 7 and 8 for $z = 0$ and 0.75, respectively. The presentation of a 3D plot has been chosen in order to show the evolution of the peak positions *versus* temperature. At room temperature the XRD patterns correspond to a mixture of monoclinic and cubic phases. Upon heating, the diffraction patterns show structures of different symmetries, which transform into a single cubic phase at high temperature. The transformation is reversible upon cooling. A comparison of the plots in Figs. 7 and 8 shows a different intermediate behavior for the two samples. Besides the structural distortion, $Y_{0.9}Gd_{0.1}Fe_2(D_{0.25}H_{0.75})_{4.1}$ displays additional reflections that are not observed for the deuteride. The evolution of the XRD pattern of $Y_{0.9}Gd_{0.1}Fe_2(D_{0.5}H_{0.5})_{4.1}$ resembles that of $Y_{0.9}Gd_{0.1}Fe_2D_{4.3}$, whereas that of $Y_{0.9}Gd_{0.1}Fe_2H_{4.4}$ is similar to the one recorded for $Y_{0.9}Gd_{0.1}Fe_2(D_{0.25}H_{0.75})_{4.1}$.

The results of the Rietveld analysis are presented in Figs. 9 and 10. Each diffraction pattern was refined using the fullprof code in order to quantify the amount of each phase, as well as their cell parameters *versus* temperature.

For $Y_{0.9}Gd_{0.1}Fe_2D_{4.3}$ (Fig. 9) the weight percentage of the monoclinic phase decreases, whereas that of the cubic phase increases above the onset temperature $T_{ons} = 328$ K. The cell parameters of the initial monoclinic phase (M) remain constant. Between 328 and 338 K, *i.e.* in the range where the T_1-T_3 DSC peaks are observed, an intermediate phase indexed in a monoclinic structure (M') with different cell parameters appears and disappears. This phase is maximum at $T_2 = 332(1)$ K. Its cell parameters a, c and β are larger than for the phase M, while b is smaller. Furthermore, the cell parameters a and c of the phase M' increase, b decreases and β increases sharply (from 122.6 to 124.0°) between 328 and 338 K. This evolution of the cell parameters corresponds to a progressive reduction of the monoclinic distortion, since the simple lowering of the crystal symmetry from a cubic to a monoclinic structure without cell distortions yields $b = c$ and $\beta = 125.265°$. Above 338 K there is only a cubic phase (C), with no clear variation of a with temperature.

Consequently, T_1 corresponds to the formation of M', T_2 to its maximum percentage and T_3 to its full transformation into the cubic structure. Upon cooling similar structural changes are observed with the appearance and disappearance of the M' phase at slightly lower temperatures than upon heating.

For $Y_{0.9}Gd_{0.1}Fe_2(D_{0.25}H_{0.75})_{4.1}$ (Fig. 10) the structural evolution from the monoclinic to the cubic phase is characterized by the presence of two new peaks at $2\theta = 30.50°$ and 33.07°, which can be indexed in an orthorhombic phase (O), isostructural to that of YFe_2H_5 (S.G. $Pmn2_1$) [27]. Upon heating, between 323 K and 330 K (between T_1 and T_3) the percentage of the monoclinic phase (M) decreases, whereas that of the cubic phase increases. The intermediate orthorhombic phase is observed in the same temperature range, with a maximum at 326 K.

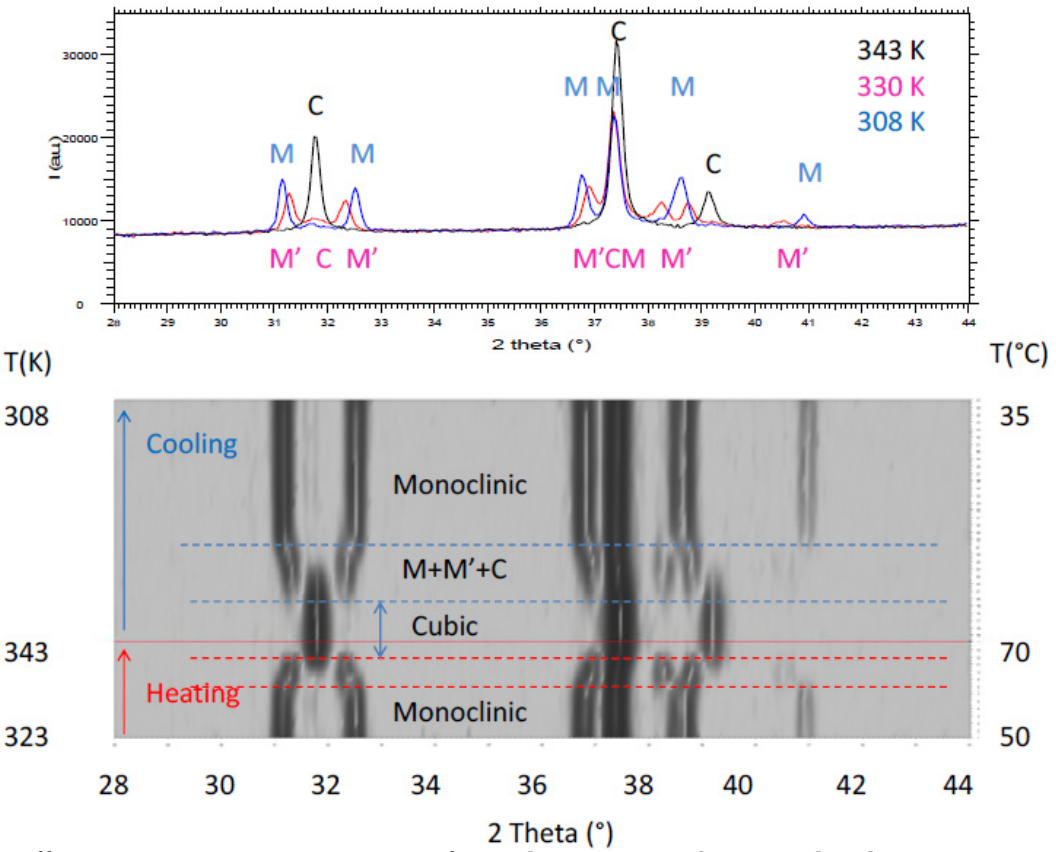

Fig. 7 Diffraction patterns *versus* temperature of $Y_{0.9}Gd_{0.1}Fe_2D_{4.3}$ upon heating and cooling.

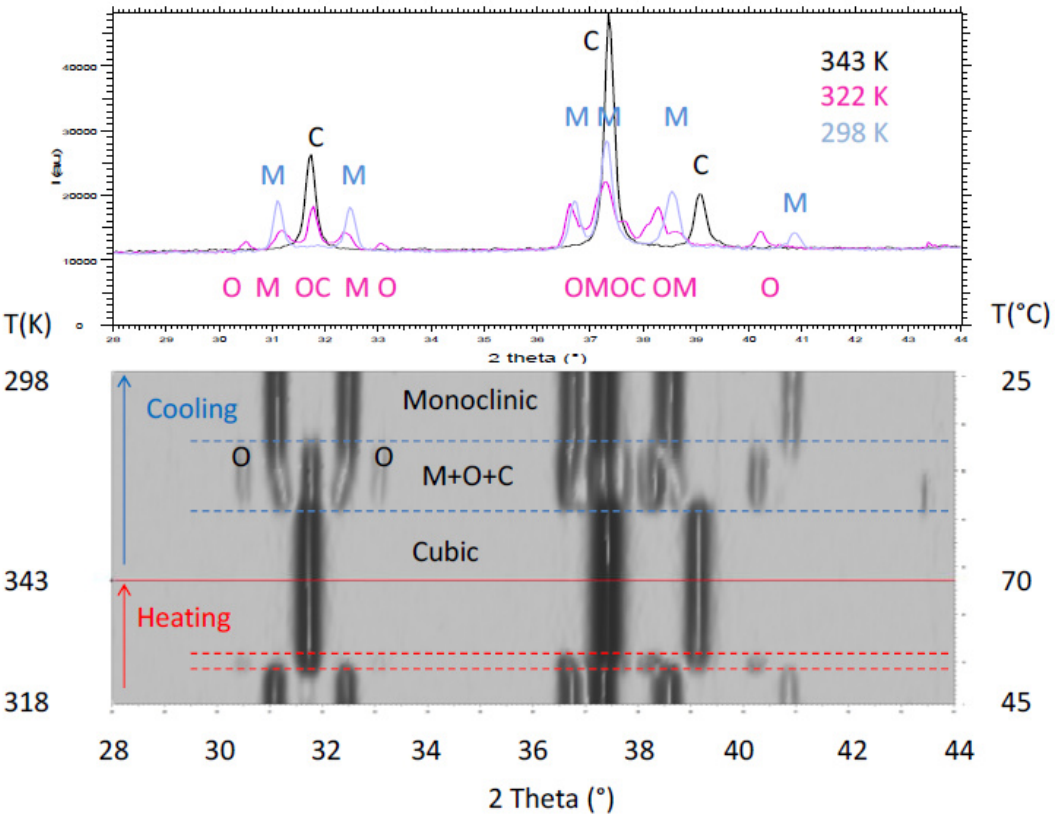

Fig. 8 Diffraction patterns *versus* temperature of $Y_{0.9}Gd_{0.1}Fe_2(H_{0.75}D_{0.25})_{4.1}$ upon heating and cooling.

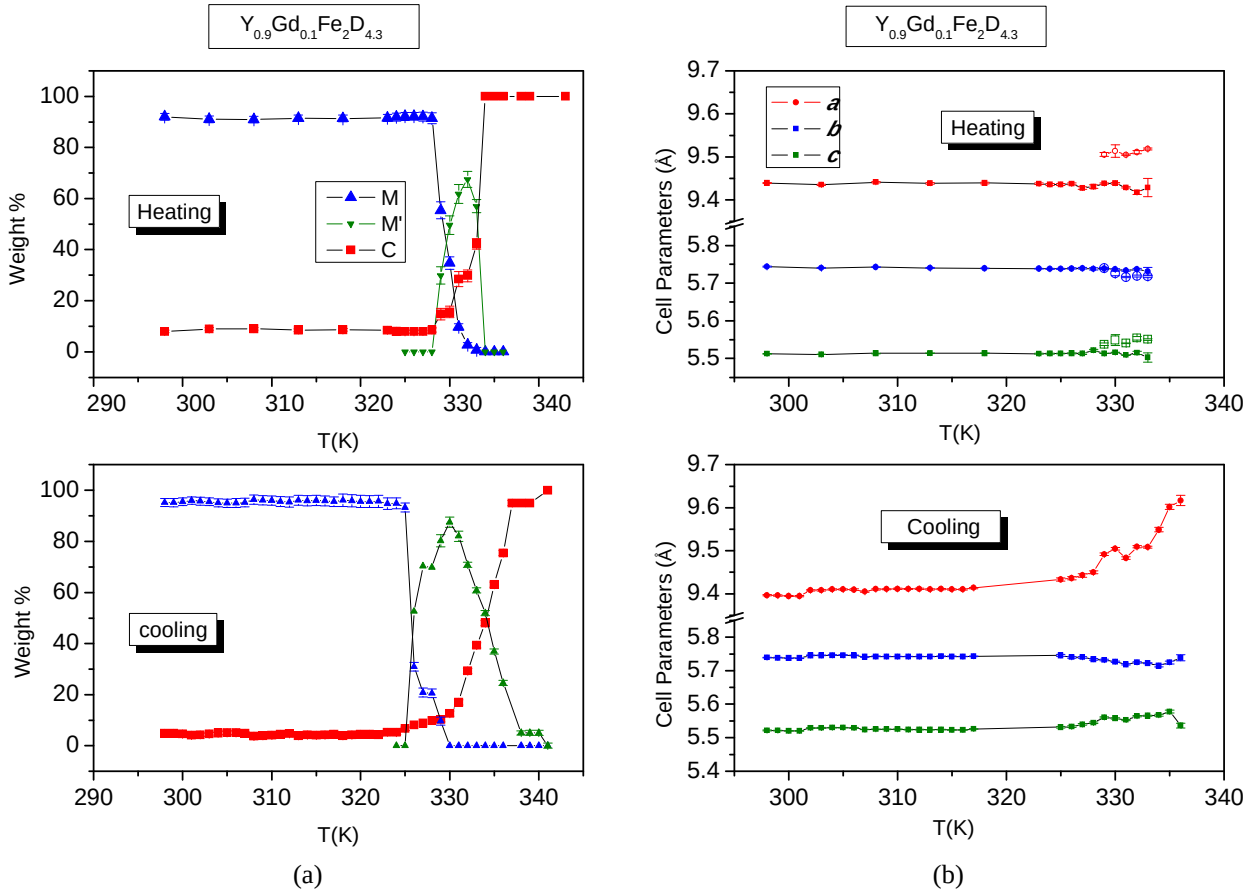

Fig. 9 Results of XRD refinement *versus* temperature for $Y_{0.9}Gd_{0.1}Fe_2D_{4.3}$ upon heating and cooling: (a) weight percent of the different phases (b) their cell parameters (full symbols correspond to the low temperature monoclinic phase and open symbols to the intermediate monoclinic phase).

Above 331 K only the cubic phase remains. Upon cooling the same sequence is observed but in a broader temperature range: the monoclinic and orthorhombic phases appear below 327 K, the orthorhombic phase is maximum at 320 K and disappears below 309 K (T_1·). Below 309 K, the percentage of monoclinic phase continues to slightly increase at the expense of the cubic phase. These temperature ranges correspond to those observed by DSC within the experimental errors.

Upon heating, the increase of *a*, *c* and *β* (122.4 to 123.6°) of the monoclinic phase and the decrease of the monoclinic *b*-parameter, as for the previous sample, are explained by a progressive reduction of the monoclinic distortion. A reversible transformation is observed upon cooling. The cell parameters of the orthorhombic phase are maximum at 320 K (for cooling), with a cell volume $V = 254.5$ Å^3. These values are nevertheless smaller than for YFe_2H_5 ($a = 5.437$ Å, $b = 5.850$ Å, $c = 8.083$ Å, $V = 257$ Å^3) [27], despite the thermal expansion and the larger cell volume due to Gd. Further studies are necessary to take into account these differences, and estimate the (H, D) content in this intermediate phase.

$Y_{0.9}Gd_{0.1}Fe_2(D_{0.5}H_{0.5})_{4.1}$ behaves like $Y_{0.9}Gd_{0.1}Fe_2D_{4.3}$, whereas $Y_{0.9}Gd_{0.1}Fe_2H_{4.4}$ shows an intermediate orthorhombic phase like $Y_{0.9}Gd_{0.1}Fe_2(D_{0.25}H_{0.75})_{4.1}$. The large difference between the transition temperatures upon heating and cooling for $z = 0.75$ and 1 therefore seems to be related to the existence of the intermediate orthorhombic phase. When the intermediate phase is monoclinic, the thermal hysteresis remains small.

iii) Thermal desorption

TGA was performed in order to check the total amount of (H, D) atoms stored in the samples and the temperature of desorption. The loss of weight due to (H, D) desorption occurs between 390 K and 550 K (Fig. 11). The derivative $\delta m/\delta T$ indicates a multipeak desorption behavior, as already observed and described for $YFe_2D_{4.2}$ [28]. The temperature maxima of the three main peaks are not very sensitive to the relative H/D content. According to the neutron powder diffraction analysis of the thermal desorption of $YFe_2D_{4.2}$, the different peaks correspond to successive phase transitions between deuterides with different

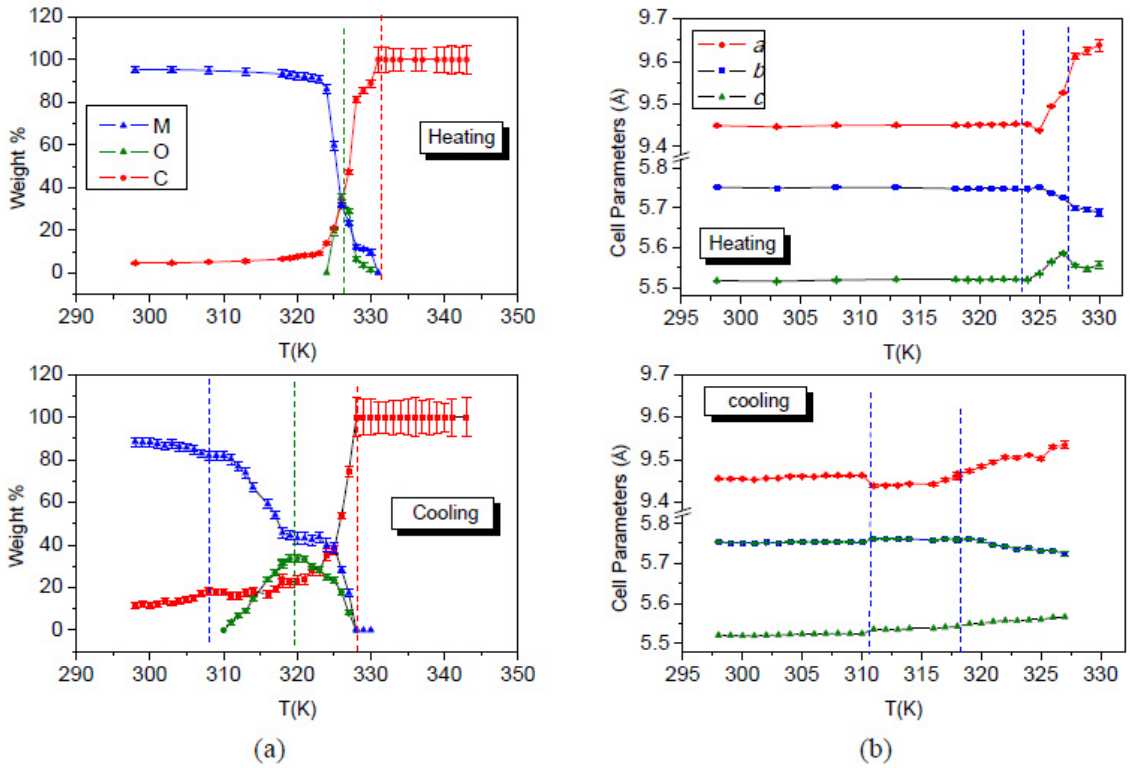

$Y_{0.9}Gd_{0.1}Fe_2(H_{0.75}D_{0.25})_{4.1}$

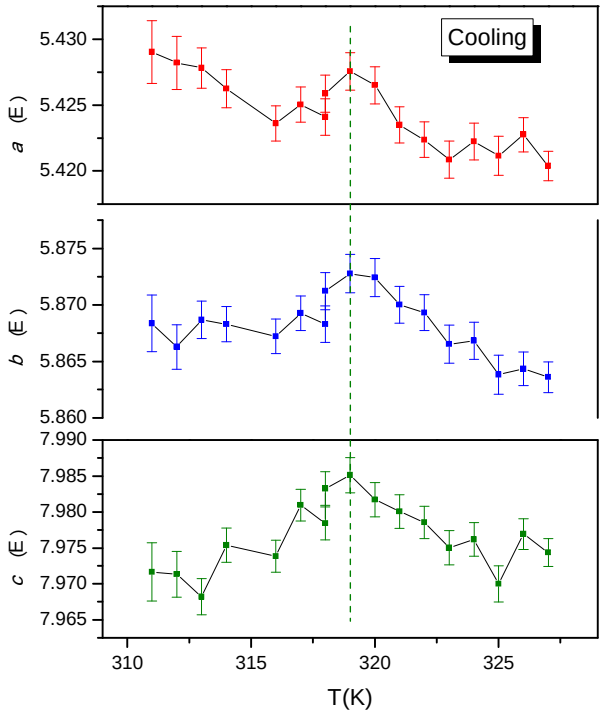

(c)

Fig. 10 Results of XRD refinement *versus* temperature for $Y_{0.9}Gd_{0.1}Fe_2(H_{0.75}D_{0.25})_{4.1}$ upon heating and cooling: (a) weight percent of the different phases, (b) cell parameters of the first monoclinic phase, (c) cell parameters of the orthorhombic phase.

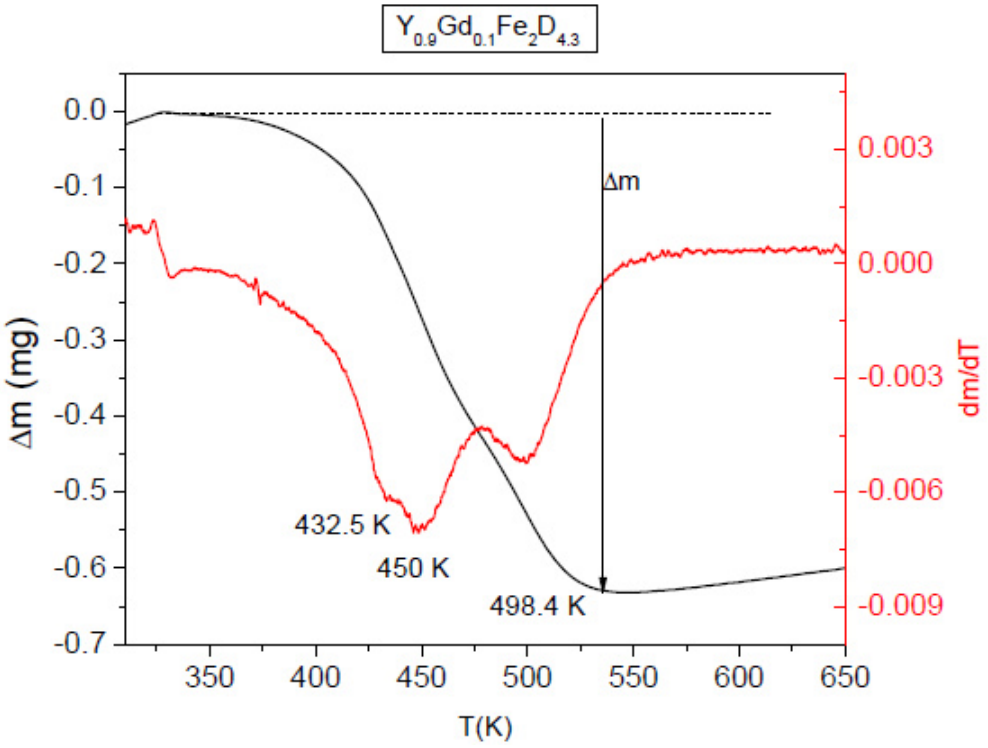

Fig. 11 Mass loss Δm (black curve) and its derivative $\delta m/\delta t$ (red curve) measured by TGA for $Y_{0.9}Gd_{0.1}Fe_2D_{4.3}$.

D contents [28]. The peak at higher temperature was attributed to the transition from $YFe_2D_{1.3}$ to YFe_2. The total capacities measured by TGA are about 0.2±0.2 (H+D)/f.u. smaller than those obtained by absorption (Table 3).

b) Band structure calculations

The equilibrium volumes after full relaxation of the YFe_2H_x compounds ($3 \leq x \leq 5$) in each structure (cubic (*Fd*-3*m*), monoclinic (*P*1*c*1) and orthorhombic (*Pmn*2_1)) are plotted in Fig. 12a. For each phase, a relative increase of the equilibrium volume is observed with increasing hydrogenation rate (x). This behavior could obviously be explained by the cell expansion induced by additional hydrogen atoms in interstitial sites. For $x > 4$, the equilibrium volumes of the three phases become very close. This behavior illustrates that each phase converges to the limit of a close packed structure, the volume corresponding to the maximum hydrogen content that may be inserted in the host compound.

The heat of formation was calculated by subtracting the weighted energy of the constituting elements in their standard element reference states from the total energy of the considered compound. In Fig. 12b, the heat of formation of each hydride is represented for the three types of structure. The cubic C15 structure appears to be the less stable phase at any hydrogenation rate. As the x rate increases, it can be seen that the most stable phase changes from the monoclinic to the orthorhombic structure, with a transition around $x = 4.5$. This is in agreement with the experimental observations for $4.0 < x \leq 5.0$. Moreover, it can be seen that for x between 4.0 and 4.5, the phase stabilities of the monoclinic and orthorhombic phase are very close ($\Delta H = 0.1$ kJ). The monoclinic phase is also more stable for $3 < x < 4$, but experimentally it is known that, around $x = 3.5$, another monoclinic phase (S.G. $P2_1/c$) appears [29]. However, no calculations have been done yet on this phase to check its stability.

The associated total magnetic moments are shown in Fig. 12c. The maximum values were obtained around $x \approx 3.5$, in agreement with the experiments [30]. Each phase presents a similar trend with a reduction of its moment with increasing hydrogen concentration, up to the disappearance of magnetic ordering for $x = 5$. This behavior has already been shown by DFT calculations [30-33] and is explained by the stability of a compound dominated by chemical metal-hydrogen interaction at this rate, which converges to a Pauli paramagnetic state.

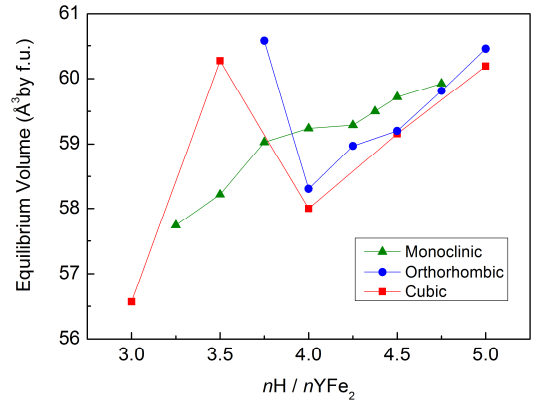

(a)

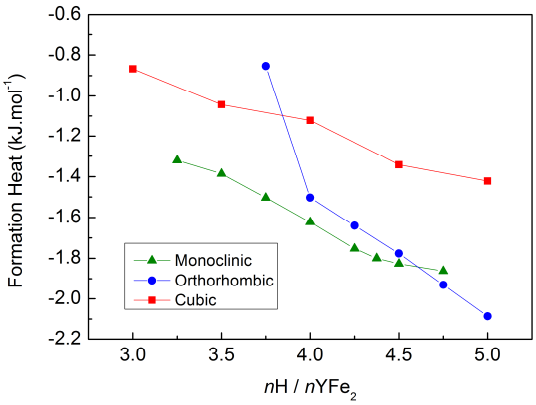

(b)

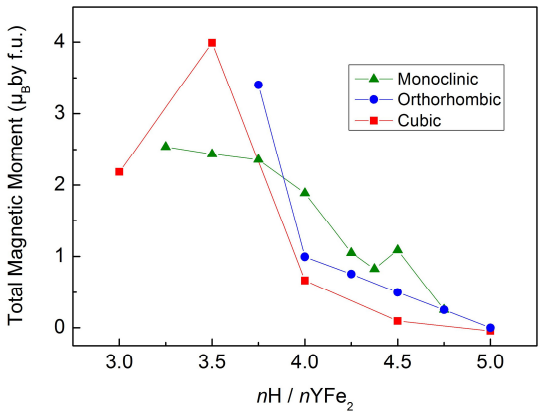

(c)

Fig. 12 Results of DFT calculations: (a) cell volume, (b) enthalpy of formation and (c) total magnetic moment for the cubic (■), monoclinic (▲) and orthorhombic (●) structures *versus* H content.

c) General discussion

In the $Y_{1-y}Gd_yFe_2$ deuterides, the H for D substitution increases $T_{F\text{-}AF}$, but decreases the order-disorder temperature from the monoclinic towards the cubic structure. The increase of $T_{F\text{-}AF}$ has already been explained by a strong magnetovolumic effect due to the cell expansion occurring upon H for D substitution [12,13].

The decrease of $T_{O\text{-}D}$ *versus* z may also result from the larger cell volume of the H-rich compounds, since $T_{O\text{-}D}$ also decreases with increasing D content in the YFe_2D_x compounds [34]. It is interesting to observe that in these $RFe_2(H,D)_x$ compounds the magnetic and the O-D transitions occur at different temperatures, , whereas the magnetic and the O-D transitions in $RMn_2(H,D)_x$ compounds occur at the same temperatures which are increasing versus x content [34-37]. The strong correlation between the magnetic and structural order in the $RMn_2(H,D)_x$ compounds has been explained by the frustration of the AF Mn sublattice in a pyrochlore structure [36,38]. This correlation can be decoupled by applying external pressure [38].

The O-D transition in the $Y_{0.9}Gd_{0.1}Fe_2(H_zD_{1-z})_{4.2(1)}$ compounds also occurs *via* an intermediate structural transformation, which is very sensitive to the (H, D) content: for the D-rich samples ($z = 0$ and 0.5) the intermediate phase is monoclinic, whereas it is orthorhombic for $z = 0.75$ and 1. The large hysteresis effect, observed between the formation and decomposition of the orthorhombic phase, probably results from the competition between two different types of H/D ordering inside the host compound. The monoclinic distortion is described in space group *C*2/*m* (12), which is a type 1 subgroup of *R*-3*m* (166), itself a type 1 subgroup of *Fd*-3*m* (227). The refinement of the neutron diffraction pattern of $YFe_2D_{4.2}$ required further lowering of the symmetry from *C*2/*m* to *Pc* (7) with doubling of the *b* parameter in order to refine all the D atom positions and occupation numbers [10]. The description of the orthorhombic structure of YFe_2D_5 requires the following subgroup sequence: *Fd*-3*m* (227) → $I4_1/amd$ (141) → *Imma* (74) → *Imm*2 (44) → $Pmn2_1$ (31) [25].

The transformation from the monoclinic to the orthorhombic phase probably requires another change of crystal symmetry, which occurs at higher temperature upon heating than upon cooling.

In $YFe_2D_{4.2}$ the O-D transition occurs *via* an intermediate structure, which was refined in the rhombohedral space group *R*-3*m* [11,13,18]. The XRD patterns *versus* temperature recorded for $YFe_2H_{4.2}$ show a similar behavior as the deuteride, without the apparition of an orthorhombic phase (unpublished work). Therefore the partial substitution of Gd for Y should play an important role to stabilize the orthorhombic structure in hydrogen-rich compounds.

The comparison of the DFT results (obtained at 0 K) with the present experiments is interesting. In fact, measurements at room temperature show that around $x \approx 4.2$ the compounds are monoclinic, in agreement with the stability found by the DFT calculations. The small difference in heat of formation between the monoclinic and the orthorhombic phases (0.1 kJ/mol) indicates the possibility of a phase transition, as observed on increasing the temperature and for Gd substitution. Gadolinium was not considered in the calculations. Actually, the YFe_2H_x cell structures considered are already large and do not allow simulating Gd substitution (which needs a supercell). Moreover, the strong localization of the *f*-electrons of Gd demands a modified exchange and correlation function, such as GGA+U, which was not considered in the present work. Gd substitution, neglected in the DFT calculations, could lower the heat of formation of the orthorhombic phase. We can assume that Gd substitution, which should increase the cell volume and induce modifications of the chemical bonds, would also affect the results presented in Fig. 12.

In the whole range of concentration, there is a large energy difference between the cubic structure and the ordered monoclinic and orthorhombic phases (0.4 kJ/mol). Since the calculations were performed at 0 K, the vibration contribution was neglected, but should be taken into account to explain the phase transitions observed at high temperature.

From the DFT calculations, a slightly larger equilibrium volume is also observed for the monoclinic structure for $x > 4$, compared to the two other phases, whereas this phase is the most stable one and could be expected to be more compact. However, from Fig. 12c it can be seen that, for $x > 4$ the monoclinic phase presents the larger magnetic moment, which induces an increase of the cell volume below $T_{F\text{-}AF}$ [10]. The larger cell volume of the monoclinic phase can result from this additional magnetostrictive effect.

Conclusion

The study of $Y_{0.9}Gd_{0.1}Fe_2(H_zD_{1-z})_x$ compounds ($x = 4.2(1)$, $z = 0$ to 1) has shown that these compounds present a very original and interesting (H, D) isotope effect. A ferromagnetic-antiferromagnetic first-order transition was observed for all the compounds, with a transition temperature increasing from 98 to 144 K for z going from 0 to 1, *i.e.* 47% increase for a cell volume change of 0.65%. These compounds also present an order-disorder structural transition from a monoclinic towards a cubic structure, with the appearance and disappearance of an intermediate phase. This intermediate phase is monoclinic for $z = 0$ and 0.5, and orthorhombic for $z = 0.75$ and 1. The transition temperatures decrease linearly *versus* z upon heating, whereas a discontinuity is observed for the low transition temperature T_1, upon cooling. The transition temperature is shifted to lower values for the samples with large H content ($z = 0.75$ and 1) and this can be explained by the presence of the orthorhombic phase.

DFT calculations agree with the experiments on the higher stability of the monoclinic phase for $x \approx 4.2(1)$, and on a change in favor of the orthorhombic phase at $x = 5$. However, the energy difference between the monoclinic and orthorhombic phase is small (0.1 kJ) and it is possible that both Gd substitution and H atoms favor the formation of the monoclinic phase upon heating. The order-disorder transition will be studied for other Gd contents in order to determine more precisely the conditions of existence of the intermediate orthorhombic phase.

Moreover, as expected, the total magnetic moment decreases with increasing x hydrogenation rate. It is difficult to consider Gd in the DFT calculations, however, the investigation of phases with lower (H, D) concentration ($x = 1.3$ to 3.5) may be interesting in order to check the phase stability for $x \leq 3.5$.

Acknowledgements

We thank E. Leroy for the microprobe analysis of the alloy. J.-C. Crivello is thankful to HPC resources from GENCI-IDRIS (Grants 2012-096175).

References

[1] G. Wiesinger, G. Hilscher, in: K.H.J. Buschow (Ed.), *Handbook of Magnetic Materials*, Elsevier North-Holland, Amsterdam, 2008, Vol. 17, p. 293.
[2] K.H.J. Buschow, A.M. van Diepen, *Solid State Commun.* 19 (1976) 79.
[3] R.M. Van Essen, K.H.J. Buschow, *J. Less-Common Met.* 70 (1980) 189.
[4] H.A. Kierstead, *J. Less-Common Met.* 86 (1982) L1.
[5] K. Kanematsu, *J. Appl. Phys.* 75 (1994) 7105.
[6] K. Kanematsu, N. Ohkubo, K. Itoh, S. Ban, T. Miyajima, Y. Yamaguchi, *J. Phys. Soc. Jpn.* 65 (1996) 1072.
[7] M. Latroche, V. Paul-Boncour, A. Percheron-Guégan, F. Bourée-Vigneron, *J. Solid State Chem.* 133 (1997) 568.
[8] V. Paul-Boncour, L. Guénée, M. Latroche, A. Percheron-Guégan, *J. Alloys Compd.* 255 (1997) 195.
[9] V. Paul-Boncour, L. Guénée, M. Latroche, A. Percheron-Guégan, B. Ouladdiaf, F. Bourée-Vigneron, *J. Solid State Chem.* 142 (1999) 120.
[10] J. Ropka, R. Cerny, V. Paul-Boncour, T. Proffen, *J. Solid State Chem.* 182 (2009) 1907.

[11] V. Paul-Boncour, G. André, F. Bourée, M. Guillot, G. Wiesinger, A. Percheron-Guégan, *Physica B* 350 (2004) e27.
[12] V. Paul-Boncour, M. Guillot, G. Wiesinger, G. André, *Phys. Rev. B* 72 (2005) 174430.
[13] O. Isnard, V. Paul-Boncour, Z. Arnold, C.V. Colin, T. Leblond, J. Kamarad, H. Sugiura, *Phys. Rev. B* 84 (2011) 094429.
[14] T. Leblond, V. Paul-Boncour, M. Guillot, O. Isnard, *J. Appl. Phys.* 101 (2007) 09G514.
[15] M. Guillot, V. Paul-Boncour, T. Leblond, *J. Appl. Phys.* 107 (2010) 09E144.
[16] V. Paul-Boncour, T. Mazet, *J. Appl. Phys.* 105 (2009) 013914.
[17] V. Paul-Boncour, T. Mazet, M. Phejar, O. Isnard, C. Colin, *Proc. Fourth IIF-IIR Int. Conf. Magnetic Refrigeration at Room Temperature*, Baotou, China, 2010.
[18] J. Ropka, R. Cerný, V. Paul-Boncour, *J. Solid State Chem.* 184 (2011) 2516.
[19] V. Paul-Boncour, G. Wiesinger, C. Reichl, M. Latroche, A. Percheron-Guégan, R. Cortes, *Physica B* 307 (2001) 277.
[20] J. Rodríguez-Carvajal, *Proc. Congr. IUCR*, 1990, p. 127.
[21] G. Kresse, J. Hafner, *Phys. Rev. B* 48 (1993) 13115.
[22] G. Kresse, D. Joubert, *Phys. Rev. B* 59 (1999) 1758.
[23] J.P. Perdew, Y. Wang, *Phys. Rev. B* 45 (1992) 13244.
[24] V. Paul-Boncour, L. Guénée, M. Latroche, M. Escorne, A. Percheron-Guégan, C. Reichl, G. Wiesinger, *J. Alloys Compd.* 253-254 (1997) 272.
[25] V. Paul-Boncour, S.M. Filipek, I. Marchuk, G. André, F. Bourée, G. Wiesinger, A. Percheron-Guégan, *J. Phys.: Condens. Matter* 15 (2003) 4349.
[26] P. Jena, C.B. Satterthwaite, *Mater. Res. Soc. Symp. Proc.* 1 (1981) 547.
[27] V. Paul-Boncour, S.M. Filipek, A. Percheron-Guégan, I. Marchuk, J. Pielaszek, *J. Alloys Compd.* 317-318 (2001) 83.
[28] T. Leblond, V. Paul-Boncour, F. Cuevas, O. Isnard, J.F. Fernandez, *Int. J. Hydrogen Energy* 34 (2009) 2278.
[29] G. Wiesinger, V. Paul-Boncour, S.M. Filipek, C. Reichl, I. Marchuk, A. Percheron-Guégan, *J. Phys.: Condens. Matter* 17 (2005) 893.
[30] V. Paul-Boncour, S. Matar, *Phys. Rev. B* 70 (2004) 184435.
[31] S.F. Matar, V. Paul-Boncour, *C. R. Acad. Sci., Ser. IIC* 3 (2000) 27.
[32] D.J. Singh, M. Gupta, *Phys. Rev. B* 69 (2004) 132403.
[33] J.C. Crivello, M. Gupta, *J. Alloys Compd.* 404-406 (2005) 150.
[34] V. Paul-Boncour, *J. Alloys Compd.* 367 (2004) 185.
[35] H. Figiel, J. Przewoznik, V. Paul-Boncour, A. Lindbaum, E. Gratz, M. Latroche, M. Escorne, A. Percheron-Guégan, P. Mietniowski, *J. Alloys Compd.* 274 (1998) 29.
[36] I.N. Goncharenko, I. Mirebeau, A.V. Irodova, E. Suard, *Phys. Rev. B* 56 (1997) 2580.
[37] I.N. Goncharenko, I. Mirebeau, A.V. Irodova, E. Suard, *Phys. Rev. B* 59 (1999) 9324.
[38] I. Mirebeau, I.N. Goncharenko, A.V. Irodova, E. Suard, *Physica B* 241-243 (1997) 672.